Editors' Suggestion | Featured in Physics

Laser-Driven Electron Lensing in Silicon Microstructures

Dylan S. Black,[1] Kenneth J. Leedle,[1] Yu Miao,[1] Uwe Niedermayer,[2] Robert L. Byer,[3] and Olav Solgaard[1]

(ACHIP Collaboration)

[1]*Department of Electrical Engineering, Stanford University, David Packard Building, 350 Serra Mall, Stanford, California 94305-9505, USA*
[2]*Institut für Theorie Elektromagnetischer Felder, Technische Universität Darmstadt, Schloßgartenstr. 8, 64289 Darmstadt, Germany*
[3]*Department of Applied Physics, Stanford University, 348 Via Pueblo Mall, Stanford, California 94305-4090, USA*

(Received 24 October 2018; published 12 March 2019)

We demonstrate a laser-driven, tunable electron lens fabricated in monolithic silicon. The lens consists of an array of silicon pillars pumped symmetrically by two 300 fs, 1.95 μm wavelength, nJ-class laser pulses from an optical parametric amplifier. The optical near field of the pillar structure focuses electrons in the plane perpendicular to the pillar axes. With 100 ± 10 MV/m incident laser fields, the lens focal length is measured to be 50 ± 4 μm, which corresponds to an equivalent quadrupole focusing gradient B' of 1.4 ± 0.1 MT/m. By varying the incident laser field strength, the lens can be tuned from a 21 ± 2 μm focal length ($B' > 3.3$ MT/m) to focal lengths on the centimeter scale.

DOI: 10.1103/PhysRevLett.122.104801

The dielectric laser accelerator (DLA) is a dielectric microstructure that harnesses the large electric fields in femtosecond-pulsed lasers to produce an electron linear accelerator with acceleration gradients orders of magnitude higher than conventional metal accelerators [1,2]. The microstructure is a subwavelength grating whose optical near field is phase matched to a propagating electron beam, thereby accelerating the electron beam. The accelerator size is commensurate with its drive wavelength; while advantageous in some respects, this presents new challenges. To confine an electron beam to a μm-scale DLA channel, a lens with focusing strength many orders of magnitude higher than currently available is necessary.

In conventional accelerators, the magnetic quadrupole is the preferred lens for charged particle focusing due to its high focusing strength, low dispersion, and linear field gradient [3]. Focusing strength is defined as $k = 1/(fL)$, where f is the focal length and L the length of the lens. The magnetic quadrupole focusing strength is $k[\mathrm{m}^{-2}] \approx 0.3B'[\mathrm{T/m}]/p[\mathrm{GeV}/c]$ [4]. It is common to compare lens strengths by their equivalent quadrupole field gradient B', and this convention is adopted throughout this Letter. The required B' for DLA is between 100–1000 kT/m, set by the resonant defocusing forces of the synchronous accelerating mode [1,5,6]. Conventional quadrupoles can achieve a B' of only 500 T/m [7–9]. The other commonly employed static-field lenses, einzel lenses [10], and solenoids [11], are also far too weak to achieve effective confinement. To realize an electron linac on-chip, a new type of lens, as proposed in Ref. [6], must be designed.

The ideal lens for DLA beam confinement would be stable, high-power, tunable, and monolithically integrable into the current architecture. Monolithic integration is especially critical, as alignment tolerances for μm-scale beam lines are measured in nanometers, and such tight alignment tolerances are only realistically accessible by use of a monolithic fabrication procedure for both lens and accelerator.

Electrodynamic lenses can provide the required focusing strength. Active plasma lenses have focusing gradients exceeding 3 kT/m [12], while plasma wakefield lensing has focusing strengths on the order of 1 MT/m [13,14]. Plasma wakefield lensing fits naturally with plasma-based accelerators [15], and provides more than sufficient focusing strength. However, integration of plasma lenses with photonic accelerators would require generation of stable plasmas on-chip that are compatible with the accelerator nanofabrication processes.

Strong lensing effects can also be derived from the optical near fields of femtosecond-pulsed lasers. Recently, a laser-driven lens with a 190 μm focal length was demonstrated by McNeur *et al.* [16], which is estimated to have an equivalent B' of 85 kT/m. The evanescent fields near a curved silicon grating generate a focusing field in the plane of the wafer. However, in single gratings there are always undesirable out-of-plane deflection forces [17]. Moreover, the curvature of the grating causes undesirable coupling of the two transverse planes, which complicates the lens implementation in a multistage accelerator design.

 © 2019 American Physical Society

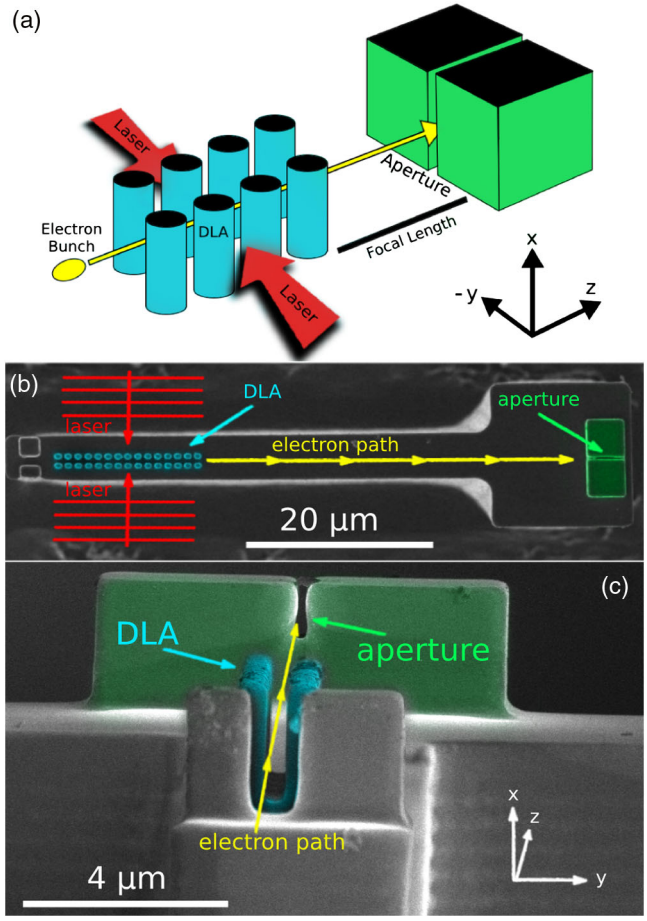

FIG. 1. (a) An electron beam passes through a DLA lens with two identical laser pulses normally incident upon it. The beam is focused, travels approximately one focal length, and is filtered by an aperture of two silicon blocks with a small gap between them. (b) An SEM of the lens and aperture, viewed from above. The lens is composed of two rows of 15 pillars each. The drift length is 39.6 μm. (c) An SEM showing the aperture structure.

In this Letter, we demonstrate a laser-driven, solid-state electron lens based on the DLA architecture, which was first proposed by Plettner *et al.* in Refs. [18,19], and whose specific architecture is discussed by Leedle *et al.* in Ref. [20]. When illuminated by two laser pulses, each with an electric field of 100 ± 10 MV/m, its focal length is measured to be 50 ± 4 μm ($B' = 1.4 \pm 0.1$ MT/m). The lens strength is continuously tunable, and we demonstrate its tuning to a focal length below 21 ± 2 μm ($B' = 3.3 \pm 0.3$ MT/m). The lensing behavior agrees well with simulation, and we provide a linearized model that approximates the lens focal length. This lens architecture adds no additional complexity to the accelerator fabrication process, as it uses identical procedures and can be integrated directly into the lithographic mask. The demonstrated focusing strength is sufficient to confine an electron beam to a μm-scale beam line. We propose that this lens be used in an alternating phase focusing (APF) scheme [6], which allows stable beam confinement and acceleration over arbitrary distances.

The lens structure (Fig. 1) is fabricated from monolithic 5–10 Ω cm B:Si, and consists of 2 rows of 15 pillars, with periodicity $\Lambda = 1013$ and a 375 nm wide channel between the rows. The pillars are elliptical (613×459 nm), with a height of 2.7 μm. The electron beam passes though the central channel, where it interacts with two 300 ± 25 fs laser pulses with a center wavelength of 1.950 ± 0.005 μm and a $1/e^2$ radius of 20 ± 2 μm. Following the lens is 39.6 μm of drift space, then an aperture consisting of two $4 \times 4 \times 2.7$ μm silicon blocks with a gap of 150 ± 10 nm between them.

The electromagnetic fields in the lens are described following Refs. [20–22]. We consider a dual-pillar structure semi-infinite in x, symmetric in y, and periodic in z. The device is illuminated by two counterpropagating z-polarized plane waves, incident from the $\pm y$ directions (Fig. 1), each with electric field E_{inc}. The electrons travel in z with velocity $\beta = v/c$. The synchronicity (or phase matching) condition between the laser field and the electron is

$$\beta\lambda_0 = \Lambda, \tag{1}$$

where λ_0 is the central laser wavelength and Λ is the structure periodicity. The Lorentz force on an electron inside the structure, assuming Eq. (1) is satisfied and non-phase-matched harmonics are negligible, is

$$\vec{F} = -\frac{qe_1}{2\gamma}\mathrm{Re}\begin{bmatrix} 0 \\ \sin\phi[(e^{i\theta}-1)\cosh(k_y y) + (e^{i\theta}+1)\sinh(k_y y)] \\ \gamma\cos\phi[(e^{i\theta}+1)\cosh(k_y y) + (e^{i\theta}-1)\sinh(k_y y)] \end{bmatrix}, \tag{2}$$

where $\gamma = (1-\beta^2)^{-1/2}$, $k_y = 2\pi/\beta\gamma\lambda_0$ is the wave vector of the evanescent field, q is the elementary charge, and e_1 is the magnitude of the synchronous accelerating field at $y = 0$ [21]. We assume a laser phase such that e_1 is purely real and positive, and define the structure constant $c_s = e_1/E_{\mathrm{inc}}$. ϕ is the phase of the electron relative to the optical cycle of the $+y$ plane wave, and θ is the relative phase between the counterpropagating waves. The force along the x coordinate is zero by the semi-infinite assumption. Previous experimental results, as well as 3D FDTD simulations, indicate that the semi-infinite approximation works well for 2.7 μm tall (or taller) pillars [20].

The magnitude of the transverse and longitudinal forces differ by a factor of γ, as expected from the Panofsky-Wenzel theorem [23].

For in-phase drive lasers ($\theta = 0$) and assuming perfect synchronicity, the focal length of a device with N periods is approximately

$$f \approx \frac{\beta^2\gamma^3 m_e c^2}{2\pi N q e_1 \sin\phi}. \tag{3}$$

Equation (3) is valid for a sufficiently small N such that the thin-lens approximation holds. The lens strengths considered here restrict the validity of Eq. (3) to devices with $N < 18$.

Neglecting phase slippage due to acceleration, valid for short structures, the energy gain in the $\theta = 0$ mode is

$$\Delta U \approx -q e_1 N \Lambda \left(\frac{\cos\theta + 1}{2}\right) \cos\phi. \tag{4}$$

For out-of-phase drive lasers ($\theta = \pm\pi$), there exists, to first order in y, a constant deflection force whose direction varies sinusoidally with ϕ. Further discussion of the accelerator modes is contained in the Supplemental Material [24].

The electron bunch is modeled as a collection of normally distributed x, y, and ϕ values. Each electron experiences a focal length drawn from the distribution of Eq. (3), and for an electron beam much longer than an optical cycle (~6 fs), the electrons within the bunch stochastically sample all possible focal lengths. To measure the minimum lens focal length, a very small aperture is placed one focal length from the lens and acts as a temporal filter, biasing electron detection towards the focusing phases ($0 < \phi < \pi$) over the defocusing phases ($\pi < \phi < 2\pi$).

The electron beam used in this experiment was produced with a 300 ± 25 fs FWHM, 100 kHz, 256 nm laser pulse incident on a flat copper cathode. The electron beam has a circular Gaussian spatial profile and a 4σ width of 780 ± 63 nm at the lens entrance, measured by a knife edge scan. The geometric 1D emittance is estimated to be ~0.5 nm rad. The beam energy is 89.4 ± 0.1 keV, which corresponds to $\beta \approx 0.525$. The beam current is set to 730 ± 200 e^-/s to avoid energy broadening from space charge effects at the cathode. Each electron pulse at the interaction point is 740 ± 110 fs FWHM in length, measured by cross correlation with a 300 ± 25 fs laser pulse.

$43 \pm 8\%$ of electrons are transmitted through the aperture with the laser (and thus the lens) off. Leakage through the silicon blocks is small; the blocks block 95% of incident electrons. For the $\theta = 0$ focusing mode, an increase in electron transmission through the aperture is expected, with maximal transmission when the drift length is matched to the lens focal length. "Contrast," the percent increase in electron transmission when the lens is turned on [Eq. (5)], quantifies this increase.

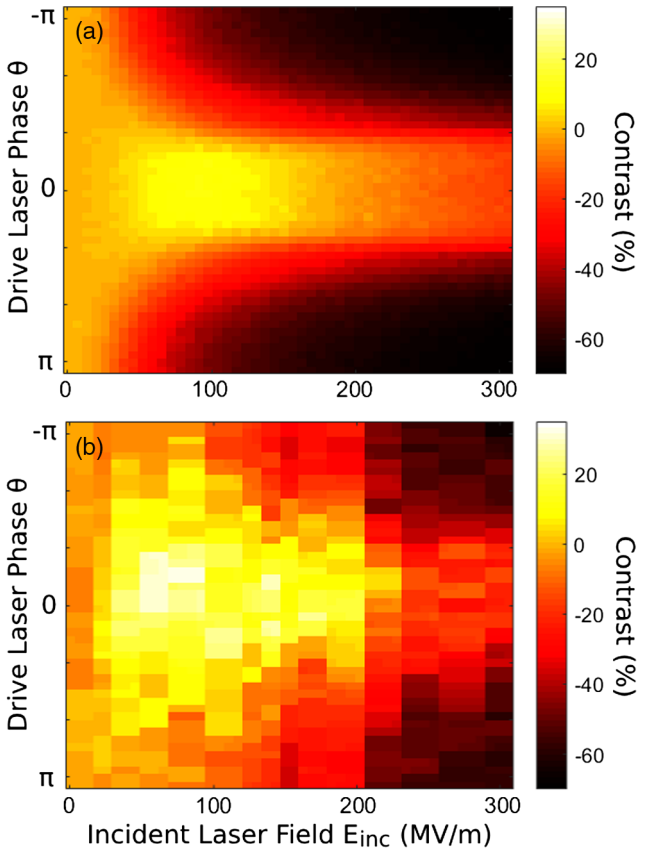

FIG. 2. (a) Simulated contrast plotted against relative drive laser phase θ and electric field E_{inc}. The simulation is a symplectic 2D particle-tracking scheme based on Ref. [21] which applies a momentum kick once per lens period equal to the time integral of Eq. (2) over one structure period. Expected contrast is calculated by a Monte Carlo approach. (b) Contrast is measured as a function of θ and E_{inc}.

$$\mathrm{Contrast}[\%] \equiv 100\left(\frac{T_{\mathrm{on}}}{T_{\mathrm{off}}} - 1\right). \tag{5}$$

T_{on} is the electron transmission with the lens on, and T_{off} is the electron transmission with the lens off. After the aperture, the electrons travel through a magnetic spectrometer with an energy resolution of 100 eV, and are detected on a microchannel plate detector.

Electron transmission simulations were carried out for a range of incident laser fields (E_{inc}) and drive laser phases (θ) [Fig. 2(a)]. Because of the long bunch length, the increased transmission from the focusing phases is partially offset by the decreased transmission from the defocusing phases. Thus, the expected contrast in this operating mode is low, only 11%. However, for the $\theta = \pm\pi$ mode, a large transmission decrease for all values of ϕ is expected.

In Fig. 2(b), the parameter space simulated in Fig. 2(a) is measured. The experimental data agree qualitatively with the simulation. There is a small contrast peak at $E_{\mathrm{inc}} = 100 \pm 10$ MV/m for $\theta = 0$, with a large region of strong negative contrast in the $\theta = \pm\pi$ region.

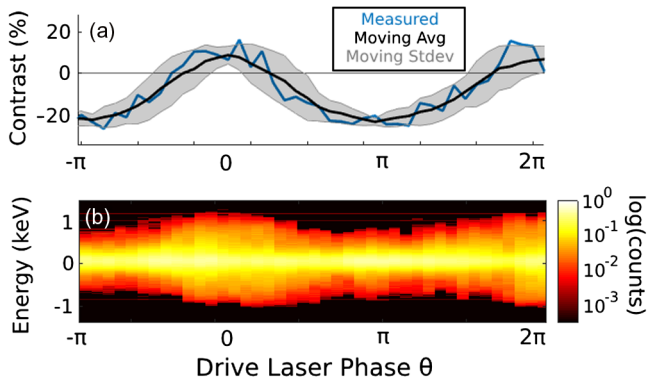

FIG. 3. (a) The measured contrast as a function of θ for $E_{\mathrm{inc}} = 137 \pm 13$ MV/m. The blue line is measured data, the black line and gray shaded area are the moving average and standard deviation, respectively. (b) The electron energy spectrum is measured simultaneously with the phase sweep in (a). Electron counts are normalized to the maximum value.

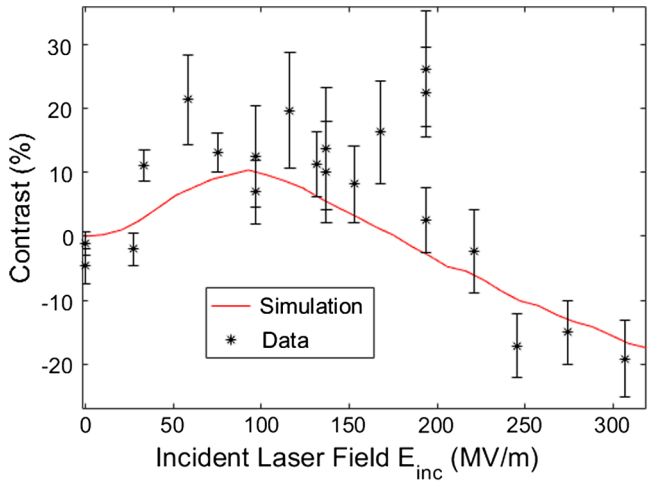

FIG. 4. This figure plots the contrast and standard deviation as a function of E_{inc} for $\theta = 0$. The simulation curve is a cross section of Fig. 2(a) at $\theta = 0$. Duplicate runs have been included.

The energy modulation and contrast as a function of drive laser phase is shown in Fig. 3. The sinusoidal variation of energy gain and contrast predicted by Eq. (4) is demonstrated, and the peak transmission and peak energy modulation occur at the same θ, in agreement with theory.

Figure 4 plots contrast in the $\theta = 0$ focusing mode as a function of E_{inc}, to aid a visual comparison between simulation and experiment. The colocation of the peak contrast for simulation and experiment is apparent. Duplicate runs omitted from Fig. 2(b) for visual clarity are included in Fig. 4.

The contrast peak at $E_{\mathrm{inc}} = 100 \pm 10$ MV/m ($e_1 = 38$ MV/m) corresponds to a focal length of 64 ± 6 μm in the linearized approximation [Eq. (3)]. Our experimentally measured focal length, defined as the total distance from the lens principal plane to aperture center, is measured to be 50 ± 4 μm ($B' = 1.4 \pm 0.1$ MT/m). The measured focal power is greater than predicted by Eq. (3), indicating that the thin-lens approximation breaks down at these lens strengths. The simulation, which uses the forces from Eq. (2), accurately predicts the incident field which gives peak contrast. Because the measured focal length will always be less than that predicted by the linearized approximation, Equation (3) can be considered a lower bound on the lens focusing strength. The incident laser field is increased to a maximum of 306 ± 16 MV/m, corresponding to a linearized focal length of 21 ± 2 μm ($B' = 3.3 \pm 0.3$ MT/m).

The structure constant c_s was measured to be 0.38 ± 0.04 for this structure, with a maximum acceleration gradient e_1 of 111 ± 6 MeV/m. Previous work with similar structures has demonstrated $c_s = 0.27 \pm 0.03$, with $e_1 = 133 \pm 8$ MeV/m [20].

The main experimental limitation was electron beam pointing instability. The electron beam could be stably aligned to the aperture for approximately 60 s, limited by thermal drifts. An averaging time of 3 s per data point (~2000 electrons) was chosen to compromise between high frequency and low frequency noise. The effects of random beam motion are partially compensated by normalizing the total number of transmitted electrons to the fraction of electrons detected at the initial beam energy of 89.4 keV. Since the laser pulse is shorter than the electron pulse, many electrons within the pulse do not interact with the laser, and these electrons are all detected at 89.4 keV. The fluctuation of the electron counts detected at 89.4 keV serves as an instantaneous measure of electron beam misalignment. The details are included in the Supplemental Material [24].

The focusing strength scales as $1/\gamma^3$, which is a less favorable scaling than the $1/\gamma^2$ scaling of solenoids or the $1/\gamma$ scaling of quadrupoles. The equivalence point is found by equating k of a quadrupole lens to k of a DLA lens and solving for γ. The equivalence point here is ~35 MeV. This can be increased by increasing either the electric field or the lens length. Efficient laser-electron interaction requires that the lens material refractive index n be greater than $1/\beta$ [25,26]. Silicon has $n \approx 3.45$ at $\lambda_0 = 2.0$ μm, corresponding to a lower limit of $\beta \approx 0.29$ (23 keV).

The lens focal length is continuously variable from approximately 20 microns to the centimeter scale. However, electron pulses of duration $\tau_p \ll \lambda_0/c$ are required for use as a single focal length lens. Fortunately, a pulse train created using the same DLA architecture [6,27] has the correct microbunch length and periodicity. The use of evanescent fields to focus electrons necessitates a narrow aperture, and so its emittance acceptance is small. The beam emittance in this lens is not conserved; however the emittance growth due to field nonlinearity is quite small. Achievable spot sizes are limited by third-order aberrations from the sinh focusing profile. Lens nonlinearities are treated more fully by Niedermayer *et al.* in Refs. [6,21].

We propose to use this lens in an alternating phase focusing confinement scheme. Briefly, lens stages are alternated with drift sections chosen to provide a specific phase offset between lens stages. For example, a drift length of one half period is equivalent to a π phase delay in ϕ, which reverses the sign of the lens focal length. If the phase offsets are chosen appropriately, it is possible to achieve stable confinement in both the transverse and longitudinal directions simultaneously, which can then be combined with high gradient acceleration, as detailed in Ref. [6]. The confinement requirements for DLA are set by the resonant defocusing forces [1,5,6], and since the defocusing forces are exactly those forces described by Eq. (2), the lensing forces presented here have precisely the same strength as the resonant defocusing itself. Thus, using this architecture, the focusing strength requirement for confinement in DLA is satisfied automatically, even for the large defocusing forces present in high-gradient accelerators [28].

In summary, we have demonstrated a laser-driven, continuously tunable electrodynamic lens with a focusing strength equivalent to those observed in plasmas [13,14] and which far exceeds any static-field lens. Its design is easily and monolithically integrable with current photonic accelerator architectures, and its strength is sufficient to confine an electron beam to an accelerator channel less than 1 μm wide for an arbitrary distance [6]. This removes a major roadblock in the development of scalable on-chip electron accelerators.

The authors wish to acknowledge the entire ACHIP collaboration for their support and guidance. This work is funded by the Gordon and Betty Moore Foundation (GBMF4744).

[1] R. Joel England *et al.*, Dielectric laser accelerators, Rev. Mod. Phys. **86**, 1337 (2014).

[2] K. P. Wootton *et al.*, Towards a fully integrated accelerator on a chip: Dielectric laser acceleration (DLA) from the source to relativistic electrons, Proc. IPAC **4744**, 2520 (2017).

[3] D. L. Smith, Focusing properties of electric and magnetic quadrupole lenses, Nucl. Instrum. Methods **79**, 144 (1970).

[4] J. Rossbach and P. Schmüser, Basic course on accelerator optics, 1993, http://inspirehep.net/record/347558/files/Cern.pdf; http://cds.cern.ch/record/247501.

[5] A. Ody, P. Musumeci, J. Maxson, D. Cesar, R. J. England, and K. P. Wootton, Flat electron beam sources for DLA accelerators, Nucl. Instrum. Methods Phys. Res., Sect. A **865**, 75 (2017).

[6] U. Niedermayer, T. Egenolf, O. Boine-Frankenheim, and P. Hommelhoff, Alternating-Phase Focusing for Dielectric-Laser Acceleration, Phys. Rev. Lett. **121**, 214801 (2018).

[7] J. Strait, Very high gradient quadrupoles, in *PACS2001, Proceedings of the 2001 Particle Accelerator Conference (Cat. No. 01CH37268)* (IEEE, Chicago, IL, 2002), Vol. 1, pp. 176–180.

[8] T. Eichner, Florian Grüner, S. Becker, Matthias Fuchs, D. Habs, R. Weingartner, U. Schramm, H. Backe, Peter Kunz, and Werner Lauth, Miniature magnetic devices for laser-based, table-top free-electron lasers, Phys. Rev. ST Accel. Beams **10**, 082401 (2007).

[9] S. Becker, M. Bussmann, S. Raith, M. Fuchs, R. Weingartner, P. Kunz, W. Lauth, U. Schramm, M. El Ghazaly, F. Grüner, H. Backe, and D. Habs, Characterization and tuning of ultrahigh gradient permanent magnet quadrupoles, Phys. Rev. ST Accel. Beams **12**, 102801 (2009).

[10] F. H. Read, A. Adams, and J. R. Soto-Montiel, Electrostatic cylinder lenses. I. Two element lenses, J. Phys. E **4**, 625 (1971).

[11] V. Kumar, Understanding the focusing of charged particle beams in a solenoid magnetic field, Am. J. Phys. **77**, 737 (2009).

[12] J. van Tilborg, S. Steinke, C. G. R. Geddes, N. Matlis, B. Shaw, A. Gonsalves, J. V. Huijts, K. Nakamura, J. Daniels, C. B. Schroeder, C. Benedetti, E. Esarey, S. S. Bulanov, N. Bobrova, P. Sasorov, and W. Leemans, Active Plasma Lensing for Relativistic Laser-Plasma-Accelerated Electron Beams, Phys. Rev. Lett. **115**, 184802 (2015).

[13] J. S. T. Ng, P. Chen, H. Baldis, P. Bolton, D. Cline, W. Craddock, C. Crawford, F. J. Decker, C. Field, Y. Fukui, V. Kumar, R. Iverson, F. King, R. E. Kirby, K. Nakajima, R. Noble, A. Ogata, P. Raimondi, D. Walz, and A. W. Weidemann, Observation of Plasma Focusing of a 28.5 gev Positron Beam, Phys. Rev. Lett. **87**, 244801 (2001).

[14] E. Chiadroni, M. P. Anania, M. Bellaveglia, A. Biagioni, F. Bisesto, E. Brentegani, F. Cardelli, A. Cianchi, G. Costa, D. Giovenale, G. Di Pirro, M. Ferrario, F. Filippi, G. Alessandro, A. Giribono, A. Marocchino, A. Mostacci, L. Piersanti, R. Pompili, and A. Zigler, Overview of plasma lens experiments and recent results at SPARC_LAB, Nucl. Instrum. Methods Phys. Res., Sect. A **909**, 16 (2018).

[15] S. Kuschel, D. Hollatz, T. Heinemann, O. Karger, M. B. Schwab, D. Ullmann, A. Knetsch, A. Seidel, C. Rödel, M. Yeung, M. Leier, A. Blinne, H. Ding, T. Kurz, D. J. Corvan, A. Sävert, S. Karsch, M. C. Kaluza, B. Hidding, and M. Zepf, Demonstration of passive plasma lensing of a laser wakefield accelerated electron bunch, Phys. Rev. Accel. Beams **19**, 071301 (2016).

[16] J. McNeur, M. Kozák, N. Schönenberger, K. J. Leedle, H. Deng, A. Ceballos, H. Hoogland, A. Ruehl, I. Hartl, R. Holzwarth, O. Solgaard, J. S. Harris, R. L. Byer, and P. Hommelhoff, Elements of a dielectric laser accelerator, Optica **5**, 687 (2018).

[17] K. J. Leedle, R. Fabian Pease, R. L. Byer, and J. S. Harris, Laser acceleration and deflection of 96.3 keV electrons with a silicon dielectric structure, Optica **2**, 158 (2015).

[18] T. Plettner, R. L. Byer, C. McGuinness, and P. Hommelhoff, Photonic-based laser driven electron beam deflection and focusing structures, Phys. Rev. ST Accel. Beams **12**, 101302 (2009).

[19] T. Plettner, R. L. Byer, and B. Montazeri, Electromagnetic forces in the vacuum region of laser-driven layered grating structures, J. Mod. Opt. **58**, 1518 (2011).

[20] K. J. Leedle, D. S. Black, Y. Miao, K. E. Urbanek, A. Ceballos, H. Deng, J. S. Harris, O. Solgaard, and R. L. Byer, Phase-dependent laser acceleration of electrons with symmetrically driven silicon dual pillar gratings, Opt. Lett. **43**, 2181 (2018).

[21] U. Niedermayer, T. Egenolf, and O. Boine-Frankenheim, Beam dynamics analysis of dielectric laser acceleration using a fast 6D tracking scheme, Phys. Rev. Accel. Beams **20**, 111302 (2017).

[22] Y. Wei, M. Ibison, G. Xia, J. D. A. Smith, and C. P. Welsch, Dual-grating dielectric accelerators driven by a pulse-front-tilted laser, Appl. Opt. **56**, 8201 (2017).

[23] W. K. H. Panofsky and W. A. Wenzel, Some considerations concerning the transverse deflection of charged particles in radiofrequency fields, Rev. Sci. Instrum. **27**, 967 (1956).

[24] See Supplemental Material at http://link.aps.org/supplemental/10.1103/PhysRevLett.122.104801 for derivations of some of the equations which appear in the main manuscript, as well as a detailed description of the data analysis methodology used to process the data that appears in the main manuscript.

[25] T. W. Hughes, S. Tan, Z. Zhao, N. V. Sapra, K. J. Leedle, H. Deng, Y. Miao, D. S. Black, O. Solgaard, J. S. Harris, J. Vuckovic, R. L. Byer, S. Fan, R. J. England, Y. Jo Lee, and M. Qi, On-Chip Laser-Power Delivery System for Dielectric Laser Accelerators, Phys. Rev. Applied **9**, 054017 (2018).

[26] M. Kozák, P. Beck, H. Deng, J. McNeur, N. Schönenberger, C. Gaida, F. Stutzki, M. Gebhardt, J. Limpert, A. Ruehl, I. Hartl, O. Solgaard, J. S. Harris, R. L. Byer, and P. Hommelhoff, Acceleration of sub-relativistic electrons with an evanescent optical wave at a planar interface, Opt. Express **25**, 19195 (2017).

[27] U. Niedermayer, O. Boine-Frankenheim, and T. Egenolf, Designing a dielectric laser accelerator on a chip, J. Phys. Conf. Ser. **874**, 012041 (2017).

[28] D. Cesar, S. Custodio, J. Maxson, P. Musumeci, X. Shen, E. Threlkeld, R. J. England, A. Hanuka, I. V. Makasyuk, E. A. Peralta, K. P. Wootton, and Z. Wu, High-field nonlinear optical response and phase control in a dielectric laser accelerator, Commun. Phys. **1**, 46 (2018).